Magnetic, charge, and bond order in the two-dimensional Su-Schrieffer-Heeger-Holstein model

Maxwell Casebolt,[1] Chunhan Feng,[2,1] Richard T. Scalettar,[1] Steven Johnston,[3,4] and G. G. Batrouni[5,6]

[1]*Department of Physics and Astronomy, University of California, Davis, California 95616, USA*
[2]*Center for Computational Quantum Physics, Flatiron Institute, 162 5th Avenue, New York, New York, USA*
[3]*Department of Physics and Astronomy, The University of Tennessee, Knoxville, Tennessee 37996, USA*
[4]*Institute for Advanced Materials and Manufacturing, The University of Tennessee, Knoxville, Tennessee 37996, USA*
[5]*Centre for Quantum Technologies, National University of Singapore, 2 Science Drive 3, 117542 Singapore*
[6]*Université Côte d'Azur, CNRS, Institut de Physique de Nice (INPHYNI), 06000 Nice, France*

(Received 8 April 2024; revised 12 June 2024; accepted 20 June 2024; published 8 July 2024)

Most nonperturbative numerical studies of electron-phonon interactions focus on model Hamiltonians where the electrons interact with a phonon branch via a single type of microscopic mechanism. Two commonly explored couplings in this context are the Holstein and Su-Schrieffer-Heeger (SSH) interactions, which describe phonons modulating the on-site energy and intersite electron hopping, respectively. Many materials, however, have multiple phonon branches that can each interact with electronic degrees of freedom in different ways. We present here a determinant quantum Monte Carlo study of the half-filled two-dimensional (bond) SSH-Holstein Hamiltonian, where electrons couple to different phonon branches via either the Holstein or SSH mechanism. We map the model's phase diagram and determine the nature of the transitions between charge-density wave, bond-order wave, and antiferromagnetic order.

DOI: 10.1103/PhysRevB.110.045112

I. INTRODUCTION

An electron interacting strongly with the lattice forms a composite quasiparticle known as a polaron [1,2]. Polarons can have large effective masses, which reflects the necessity of rearranging the lattice degrees of freedom as the electron moves [1–4]. If two electrons are present, they can bind together in a bipolaron, which allows one electron to take advantage of the distortion produced by the other to occupy the same region of space. At half filling and on a bipartite lattice, (bi)polarons tend to arrange themselves spatially into insulating charge-density-wave (CDW) or bond-order-wave (BOW) patterns, depending on the microscopic nature of the electron-phonon (e-ph) coupling [5–13]. For the Holstein interaction, for example, bipolarons tend to freeze into an ordered $\mathbf{Q} = (\pi/a, \pi/a)$ lattice in two dimensions (where a is the lattice constant) leading to a CDW insulating phase. Conversely, for the bond Su-Schrieffer-Heeger (SSH) interaction [14] on a single-band lattice, antiferromagnetic (AFM) order can accompany BOW owing to a positive effective intersite exchange J that appears when the phonons are integrated out [10,13,15]. However, optical SSH interactions on a multiorbital Lieb or perovskite lattice can lead to a bipolaron lattice, like in the Holstein model, for certain parameter regimes and filling values [8,12].

The thermal and quantum phase transitions to these various ordered phases have mostly been studied via quantum Monte Carlo (QMC) for each interaction in isolation, i.e., for either a Holstein coupling of the electron density to the phonon displacement [5,9,16–26] or an SSH coupling [8,10–13,15,27–31] in which the phonon modulates the intersite hopping (kinetic energy), but not both. Yet in real materials with complex unit cells, several phonon branches can couple to the electrons. Moreover, the microscopic coupling mechanism to individual branches can be different, leading to opposing effects. The high-T_c superconducting cuprates provide an interesting case in point. In these materials, the presence of a crystal field across the CuO_2 plane introduces an on-site coupling to the bond-buckling optical oxygen models [32,33]. At the same time, the bond-stretching Cu-O modes (the so-called half- and full-breathing modes) modulate the Cu-O hopping integral t_{pd} [33,34]. The former coupling is naturally described by a Holstein-like interaction, while the latter is of the SSH type. When multiple coupling mechanisms are present, one naturally expects rich competition between the ordered phases created by the respective interactions.

Despite this relevance of multibranch models to real materials, combined SSH-Holstein (SSHH) models have previously been studied via QMC only in one dimension [35]. In this case, the lower dimension precludes long-range order at nonzero temperature, resulting in ground state correlations with a power-law decay with increasing distance. The key features of the one-dimensional (1D) phase diagram are the presence of a metallic phase (spuriously absent in the pure 1D SSH model) when the Holstein coupling is introduced, and a competition between BOW and CDW correlations as the associated e-ph couplings are varied [35]. There is a direct and continuous transition between the states at strong coupling while a Luther-Emery metallic phase, in which the doublons and high kinetic energy bonds are disordered, intervenes at weak coupling where the interactions compete. The 1D SSHH model has also recently been studied in the context of designing topological analogs to magnetic bits [36].

Here, we study the two-dimensional (2D) single-band SSHH model defined on a square lattice, sketched in the lower right of Fig. 1, using determinant quantum Monte Carlo

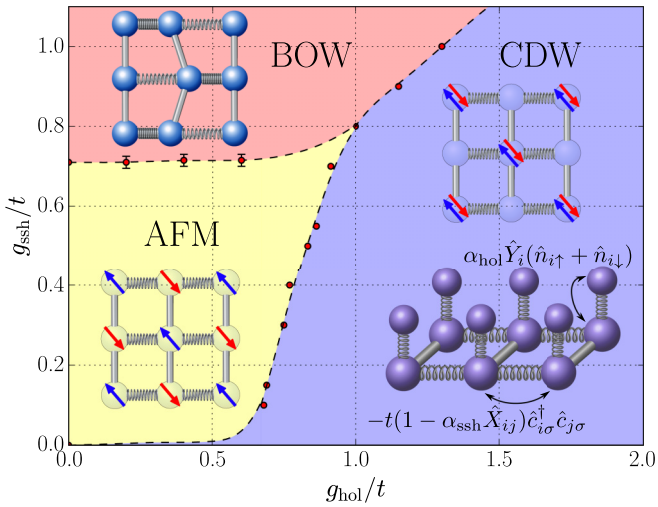

FIG. 1. The low-temperature ($T = t/16$) phase diagram of the SSH-Holstein model. Charge-density wave (CDW) order is present at any $g_{\rm hol}$ for $g_{\rm ssh} = 0$. The bond-order wave (BOW) dominates at large $g_{\rm ssh}$. For $g_{\rm ssh} \leqslant 0.7t$, antiferromagnetic (AFM) order is present for low Holstein couplings in place of BOW. Bottom right (in the blue zone): A sketch of the SSH-Holstein model. The SSH interaction couples to the electron hopping, while the Holstein interaction couples to the electron density. SSH phonons exist on lattice bonds while Holstein phonons exist on site.

(DQMC). Our main result is the low-temperature phase diagram shown in Fig. 1. It exhibits transitions between $\mathbf{Q} = (\pi/a, \pi/a)$ CDW, BOW, and AFM orders depending on the relative strengths of the SSH and Holstein couplings, $g_{\rm ssh}$ and $g_{\rm hol}$. In what follows, we will discuss the various numerical measurements leading to this phase diagram. Our results highlight the rich physics contained in *e*-ph models when one allows for coupling to multiple phonon branches, which may be relevant for understanding different classes of materials such as the transition metal oxides.

II. MODEL AND METHODS

We will compute the equilibrium properties of the "bond" SSHH model, where the in-plane phonon modes live on the links connecting pairs of sites [14] and the Holstein modes live on the sites themselves. We consider a 2D square lattice with $N = L^2$ sites, where L is the linear size of the lattice. The Hamiltonian is

$$\begin{aligned}\mathcal{H} = &-t\sum_{\langle i,j\rangle,\sigma}(1-\alpha_{\rm ssh}\hat{X}_{ij})(\hat{c}^\dagger_{i\sigma}\hat{c}_{j\sigma}+{\rm H.c.}) - \mu\sum_{i,\sigma}\hat{n}_{i\sigma}\\ &+\sum_{\langle i,j\rangle}\left(\frac{\hat{P}^2_{ij}}{2M_{\rm ssh}}+\frac{M_{\rm ssh}}{2}\omega^2_{\rm ssh}\hat{X}^2_{ij}\right)\\ &+\alpha_{\rm hol}\sum_{i,\sigma}\hat{Y}_i\hat{n}_{i\sigma}+\sum_i\left(\frac{\hat{\Pi}^2_i}{2M_{\rm hol}}+\frac{M_{\rm hol}}{2}\omega^2_{\rm hol}\hat{Y}^2_i\right). \quad (1)\end{aligned}$$

Here, $\hat{c}^\dagger_{j\sigma}$ ($\hat{c}_{j\sigma}$) are fermionic creation (destruction) operators at site j and with spin σ, t is the nearest-neighbor hopping integral, and μ is the chemical potential. The model includes two types of *e*-ph interactions: an on-site Holstein coupling $g_{\rm hol}$ to the fermionic density, and the SSH coupling $g_{\rm ssh}$ to the intersite hopping. The SSH *e*-ph coupling in units of energy $g_{\rm ssh}$ is defined as $g_{\rm ssh} = \alpha_{\rm ssh}\sqrt{\hbar/(2M_{\rm ssh}\omega_{\rm ssh})}$; the Holstein coupling $g_{\rm hol}$ can be defined similarly with its accompanying parameters. $\hat{X}_{ij}$ and $\hat{Y}_i$ are independent SSH and Holstein phonons defined on the bonds and sites, respectively. The associated momentum operators for these phonons are $\hat{P}_{ij}$ and $\hat{\Pi}_i$, respectively. The effective masses are taken to $M_{\rm ssh} = M_{\rm hol} = 1$, and the SSH and Holstein branches are dispersionless with energies $\omega_{\rm ssh}$ and $\omega_{\rm hol}$, respectively. Throughout, we set $t = 1$ as our unit of energy, and adopt $\omega_{\rm hol} = \omega_{\rm ssh} = t$. This choice fixes the adiabatic ratio $\omega_{\rm ssh}/E_{\rm F} = \frac{1}{4}$ ($E_{\rm F} = 4t$ is the Fermi energy for the half-filled band) for both sets of modes and facilitates direct comparisons of the coupling strengths $g_{\rm hol}$ and $g_{\rm ssh}$. Finally, we fix $\mu = -2g^2_{\rm hol}/\omega_{\rm hol}$ to maintain half filling.

We study Eq. (1) using DQMC [37,38]. This method expresses the finite temperature SSHH partition function as a path integral over the space and imaginary-time dependent phonon fields $X_{ij}(\tau)$ and $Y_i(\tau)$. The fermionic degrees of freedom, which appear quadratically in the Hamiltonian, are traced out analytically, so that the weight for the phonon paths is a product of a bosonic contribution originating in the pure phonon terms of Eq. (1) and a product of fermionic determinants of each spin species. The configurations of these fields are then sampled stochastically through a combination of local moves at a single imaginary time value of each field $[X_{ij}(\tau), Y_i(\tau)]$, and global moves that change the field at all imaginary-time values τ simultaneously at a single spatial site i or bond [39]. (The latter effectively samples configurations that are strongly correlated in the imaginary-time direction due to the kinetic energy terms $\hat{P}^2_{ij}$ and $\hat{\Pi}^2_i$ in the Hamiltonian.) The algorithm scales as the cube of the number of spatial sites, and (roughly) linearly with inverse temperature β. Importantly, there is no sign problem in our model at any filling [40–42] owing to the symmetric coupling of the up and down fermionic species to the phonons.

All runs begin with a "seed input," in which phonon variables have a structure similar to the expected BOW or CDW phase, based on the relative values of the *e*-ph couplings $g_{\rm hol}$ and $g_{\rm ssh}$. This practice helps reduce the number of warm-up sweeps that are needed to reach thermal equilibrium. Our code then runs through 320 imaginary time slices of $\beta = 16/t$ ($\Delta\tau = 0.05/t$) for a total of around 10^5 steps.

We characterize the SSHH model by measuring the equilibrium structure factors associated with the different types of order. The relevant real-space correlation functions are $C_\alpha(\mathbf{r}) = \sum_{\mathbf{i}}\langle O_\alpha(\mathbf{r}+\mathbf{i})O_\alpha(\mathbf{i})\rangle$, where $O_s(\mathbf{r}) = n_{\mathbf{r},\uparrow} - n_{\mathbf{r},\downarrow}$, $O_c(\mathbf{r}) = n_{\mathbf{r},\uparrow} + n_{\mathbf{r},\downarrow}$, and $O_{bx}(\mathbf{r}) = (c^\dagger_{\mathbf{r}+\hat{x},\sigma}c_{\mathbf{r},\sigma} + {\rm H.c.})$ for spin (s), charge (c), and bond kinetic energy in the $\hat{x}$ direction (bx, with an analogous definition of C_{by}), respectively. The corresponding structure factors are obtained by a Fourier transform $S_\alpha(\mathbf{q}) = \frac{1}{N}\sum_{\mathbf{r}} e^{i\mathbf{q}\cdot\mathbf{r}}C_\alpha(\mathbf{r})$. Note, our normalization is such that the structure factors are lattice size independent in high-temperature phases (short-range spatial correlations), but grow linearly with N with the onset of long-range order. We will also present results for other standard observables such as the average electron and phonon energies, double occupancy, etc. Additional details can be found in the Appendixes.

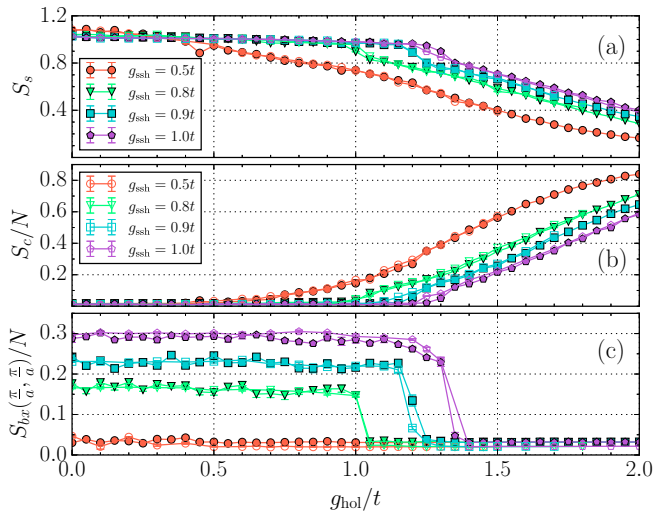

FIG. 2. (a) AFM S_s, (b) CDW S_c, and (c) BOW S_{bx} structure factors vs Holstein coupling $g_{\rm hol}$ at inverse temperature $\beta = 16/t$, and half filling for $L = 8$ (solid symbols) and $L = 10$ (open symbols). An abrupt collapse of bond order occurs as $g_{\rm hol}$ grows for SSH couplings above the critical value, accompanied by a decrease in AFM order, and a rise in CDW order. Error bars are present, but smaller than marker size.

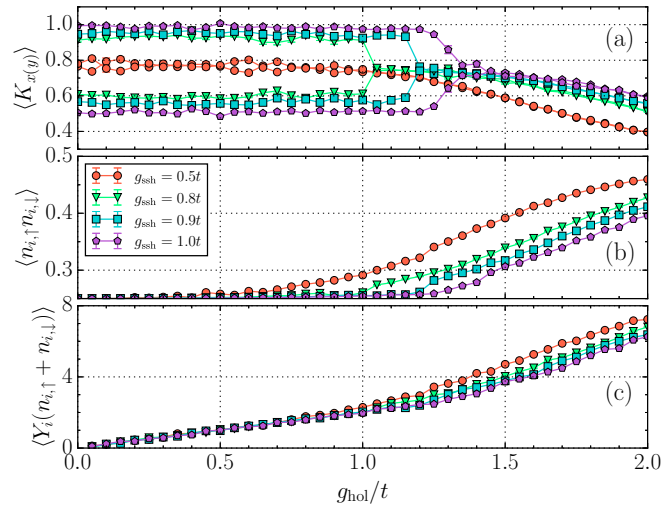

FIG. 3. (a) x/y kinetic energy, (b) double occupancy, and (c) Holstein electron-phonon coupling on an $L = 8$ system at half filling. Electronic kinetic energy and double occupancy are close to constant in the low $g_{\rm hol}$ regime where AFM order is expected for $g_{\rm ssh} \lesssim 0.7t$ and BOW are expected for $g_{\rm ssh} \gtrsim 0.7t$.

III. RESULTS

To determine the phase boundaries shown in Fig. 1, we measured the evolution of the relevant structure factors in the $(g_{\rm hol}, g_{\rm ssh})$ plane. Figure 2 plots results for the AFM [S_s, Fig. 2(a)], CDW [S_c, Fig. 2(b)], and BOW [S_{bx}, Fig. 2(c)] structure factors for a family of fixed $g_{\rm ssh}$ while sweeping $g_{\rm hol}$ from weak to strong coupling. These results were obtained at a fixed temperature $T = t/16$, which is low enough that the structure factors reflect the ground state properties of the system for our parameters, i.e., the correlation length of the order in question exceeds the linear lattice size.

Focusing first on small $g_{\rm hol}$, we find that the model is dominated by BOW order for $g_{\rm ssh} > g_{\rm ssh,c} \approx 0.7t$. This is reflected in the large value of S_{bx} at small $g_{\rm hol}$, which grows in proportion to lattice size so that S_{bx}/N is independent of N, indicative of long-range bond order.

As $g_{\rm hol}$ increases, S_{bx} undergoes an abrupt collapse, suggesting a first-order phase transition. The value of the critical $g_{\rm hol,c}$ decreases as $g_{\rm ssh}$ goes down, as does the amplitude of S_{bx}. At the same time, the strength of the CDW begins to increase continuously with $g_{\rm hol}$ once the BOW order has collapsed, as shown in Fig. 2(b). With the formation of CDW correlations, there is also a concomitant drop in the electron kinetic energy [Fig. 3(a)], increase in the double occupations [Fig. 3(b)], and a change in slope of the e-ph Holstein interaction energy [Fig. 3(c)]. These results show that hopping is rapidly phased out in favor of ordered double occupancy as the Holstein coupling begins to dominate. This behavior is very similar to the formation of CDW order in the pure 2D Holstein model [5,7,9,17,18,20–23,43–47].

These $g_{\rm ssh} \gtrsim 0.7t$ results demonstrate the presence of a first-order transition between a BOW and a CDW phase as a function of $g_{\rm hol}$ at large $g_{\rm ssh}$. However, the situation is quite different at lower values of $g_{\rm ssh}$. In the pure bond-SSH model, there is a phase transition from AFM order to BOW as the value of $g_{\rm ssh}$ increases [11]. AFM is stabilized in this model because the electrons can only simultaneously tunnel on a modulated bond if they are of opposite spin [11]. This mechanism is in contrast to the AFM order found in the Hubbard model, in which on-site repulsion U penalizes double occupancy while favoring the residual exchange interaction arranging sites antiferromagnetically.

The AFM order for small $g_{\rm ssh}$ in the pure SSH model persists in the SSHH model for small $g_{\rm hol}$. For example, for $g_{\rm ssh} = 0.5t$ and small $g_{\rm hol}$ we remain in a state characterized by a higher magnitude of electronic kinetic energy accompanied by a weakly enhanced spin correlation S_s [Fig. 2(a)]. In this case, the AFM correlations are weak because the bonds are only weakly disturbed at small $g_{\rm ssh}$. Upon increasing either $g_{\rm ssh}$ or $g_{\rm hol}$, the AFM state gives way to BOW or CDW order. The CDW phase boundary has a change in slope at $g_{\rm hol} \sim t$. This corresponds well to where the extrapolation of the AFM-BOW boundary intersects the CDW phase, demonstrating further consistency between the different order parameter measurements.

Figure 3 plots several other relevant observables for the same parameter sets. The BOW order breaks the x/y symmetry on a square lattice, since alternating large and small kinetic energy bonds select one of these axes along which to align. This phenomenon is evidenced in Fig. 3(a). For $g_{\rm ssh} \geqslant 0.8t$ and small $g_{\rm hol}$, the system is in a BOW state and the kinetic energies along the x and y directions have two distinct values (differing by up to a factor of 3). Increasing $g_{\rm hol}$ causes this bifurcation to collapse as the system transitions from the BOW phase to the CDW phase. For $g_{\rm ssh} = 0.5t$, there is no BOW at any $g_{\rm hol}$ and the x and y kinetic energies are equal across this cut through the phase diagram.

Having described the phase transitions which occur at fixed $g_{\rm ssh}$ with increasing $g_{\rm hol}$ (horizontal sweeps in Fig. 1) we can

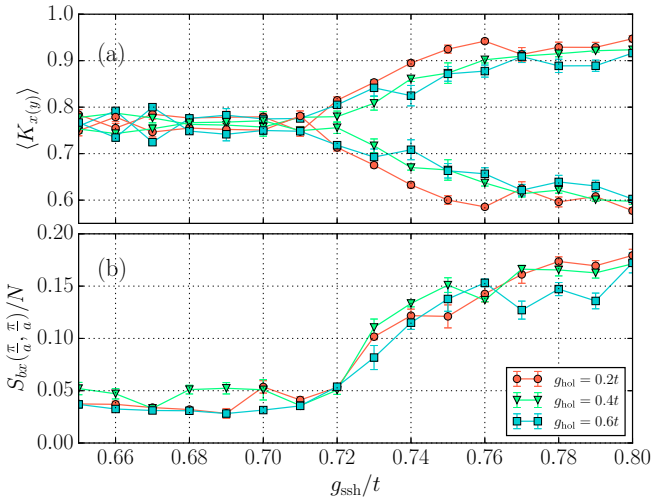

FIG. 4. (a) x/y kinetic energy and (b) BOW S_{bx} vs $g_{\rm ssh}$. Antiferromagnetic order feeds into BOW formation, transitioning at around $g_{\rm ssh,c} = 0.71t - 0.72t$.

complete our picture of the phase diagram by studying vertical sweeps in Fig. 1, i.e., trajectories at fixed $g_{\rm hol}$ with increasing $g_{\rm ssh}$. These are given in Fig. 4. The expected transition into a BOW phase is confirmed by a sharp rise in S_{bx} [Fig. 4(b)] and a kinetic energy bifurcation [Fig. 4(a)]. The critical value of $g_{\rm ssh}$ is almost independent of $g_{\rm hol}$, reflecting the nearly horizontal AFM-BOW boundary of Fig. 1.

IV. CONCLUSIONS

We have mapped the low-temperature phase diagram of the 2D SSHH model at half filling in the $(g_{\rm hol}, g_{\rm ssh})$ plane. Starting in an AFM phase found at weak couplings, we found that increasing $g_{\rm ssh}$ up to a critical value results in x/y symmetry breaking as the intersite hopping modulates into a regular pattern, creating a BOW. For every value of $g_{\rm ssh}$, however, a critical value of $g_{\rm hol}$ exists that destroys the BOW and replaces it with a CDW. We find that the enhancement of BOW at higher $g_{\rm ssh}$ delays the CDW onset (i.e., requiring larger $g_{\rm hol}$); this behavior is due to the direct competition between the phases, as BOW favors quantum fluctuations and CDW prefers electron localization. In many models with competing interactions, e.g., the 1D extended Hubbard Hamiltonian [48–50], the transition between different phases changes from second order at weak coupling to first order at strong coupling. We do not see firm evidence for such a tricritical point here. However, it is possible we are not yet at strong enough coupling. The largest value of the effective (attractive) $U_{\rm eff} = -2g_{\rm hol}^2/\omega_{\rm hol}$ in our phase diagram of Fig. 1 is $|U_{\rm eff}| \sim 2t$. The strong-coupling (first-order) character in the 1D extended Hubbard model occurs only beyond $(U_t, V_t) = (5.89t, 3.10t)$ [51], and would likely require even larger values in the 2D geometry studied here.

Our work parallels exploration of the interplay of individual forms of e-ph interaction with on-site electron-electron interactions (a Hubbard U) [7,39,52]. In the case of the Hubbard-SSH Hamiltonian at half filling there is no fermion sign problem [31,40–42] and the low-temperature antiferromagnetic to BOW phase can be effectively characterized [11]. As this work was done entirely for $\beta = 16/t$, a fruitful investigation would be to characterize the transition temperatures between the AFM and BOW transitions in the presence of Holstein phonons.

ACKNOWLEDGMENTS

This work was supported by the U.S. Department of Energy, Office of Science, Office of Basic Energy Sciences, under Award No. DE-SC0022311. The Flatiron Institute is a division of the Simons Foundation.

APPENDIX A: AVERAGE FILLING VERSUS CHEMICAL POTENTIAL

Figure 5 plots the average site occupation $\langle n \rangle = \frac{1}{N}\sum_{i,\sigma}\langle c_{i,\sigma}^\dagger c_{i,\sigma}\rangle$ as a function of the chemical potential μ for three representative points in the $(g_{\rm ssh}, g_{\rm hol})$ phase diagram. Specifically, curves are shown in the AFM $(t/2, 0)$, CDW $(0, 1.2t)$, and BOW $(t, 0)$ phases. All three curves show a plateau around half filling, indicating that each phase has a gap in their single-particle energy spectrum. In other words, they are insulating. One may notice the sharper approach to the CDW plateau in Fig. 5(b), a feature that has also been reported in Fig. 7 of Ref. [23].

The plateaus of CDW/BOW order [Figs. 5(b) and 5(c)] are longer than that of AFM order. This is due to the types of symmetries being broken in such regions: continuous for AFM order, and discrete for CDW/BOW order. While continuous symmetry breaking is forbidden in two dimensions, the correlation length ξ grows as $e^{1/T}$; at sufficiently low temperatures such as $T = t/16$, the correlation length has outpaced the system size L, allowing us to access effectively zero-T physics.

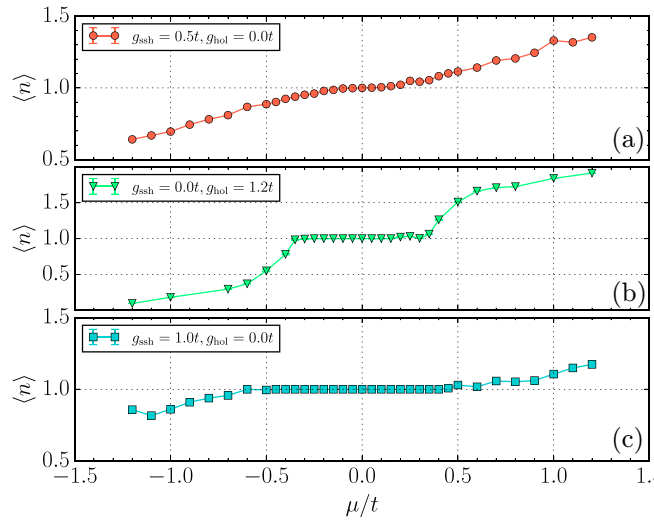

FIG. 5. The average site density $\langle n \rangle$ as a function of the chemical potential μ at $\omega_{\rm ssh} = \omega_{\rm hol} = t$, recorded in three representative points $(g_{\rm ssh}, g_{\rm hol})$ of the phase diagram: (a) AFM, (b) CDW, and (c) BOW. A shift in the half-filling value of μ is present via $-\frac{2g_{\rm hol}^2}{\omega_{\rm hol}}$, and these plots have been shifted by said amount to coincide with half filling at $\mu = 0$.

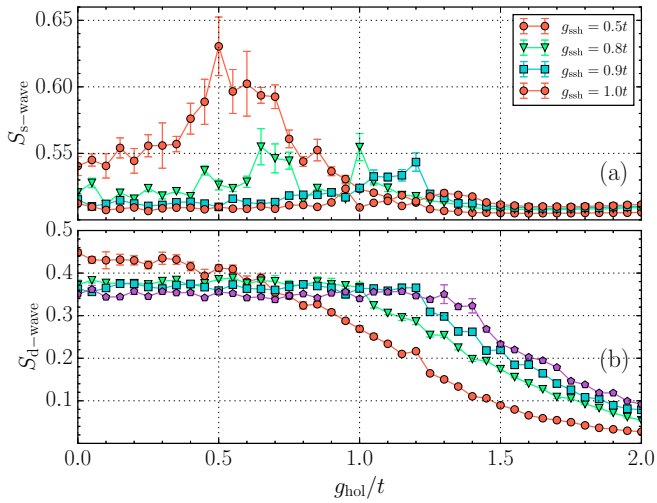

FIG. 6. Pairing structure factor $S_{s\text{-wave}}$ (a) and $S_{d\text{-wave}}$ (b) as functions of Holstein coupling g_{hol} for four fixed values of g_{ssh}. The s-wave structure factor has a peak at the AFM-CDW boundary, though the value is too small to be associated with long range order. The d-wave structure factor is everywhere small (short ranged in real space), but it is largest in the AFM phase. This parallels the known connection between spin-density-wave order and d-wave pairing in the Hubbard model.

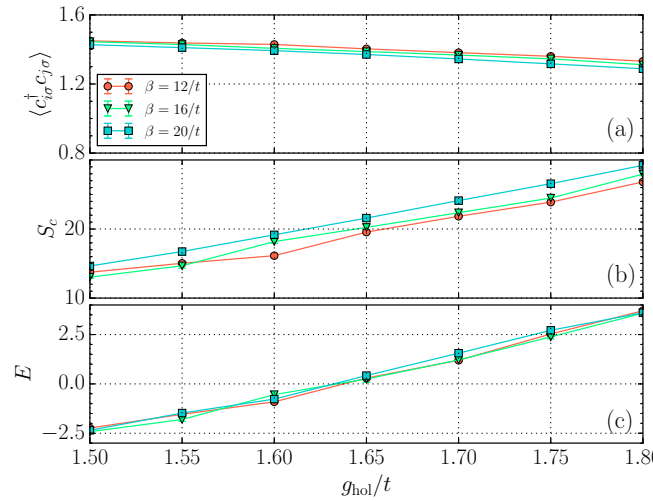

FIG. 7. Kinetic energy (a), charge structure factor S_c (b), and total energy (c) for $\beta = 12/t$, $16/t$, and $20/t$. The SSH coupling $g_{\text{ssh}} = 1$. Since the data for $\beta = 16/t$ and $\beta = 20/t$ coincide, we conclude $\beta = 16/t$ is sufficiently large to be sampling the properties of the ground state.

APPENDIX B: SUPERCONDUCTING CORRELATIONS

Figure 6(a) shows the s-wave pairing structure factor, $S_{s\text{-wave}}$, at different fixed g_{ssh} as a function of g_{hol}. The Holstein model itself has a CDW ground state at half filling ($\langle n \rangle = 1$), and supports superconductivity when doped [23,53]. Therefore, we interpret the peak in $S_{s\text{-wave}}$ to be associated with loss of the competing CDW correlations once $g_{\text{ssh}} \gtrsim g_{\text{hol}}$.

In the Hubbard model, d-wave superconductivity is associated with AFM correlations, which are strongest near half filling. Given the presence of weak AFM correlations in the bond SSH model [10,13,15], it is then natural to wonder whether similar unconventional pairing can appear in our model. To explore this possibility, Fig. 6(b) shows the pairing structure factor $S_{d\text{-wave}}$ at different fixed g_{ssh} and increasing g_{hol}. We observe that $S_{d\text{-wave}}$ turns downward to lower values once the system exits the AFM phase and enters the CDW phase. Likewise, comparing the plots for increasing g_{ssh}, we see that $S_{d\text{-wave}}$ falls as the BOW phase is approached. Thus there appears to be a correlation between d-wave pairing and AFM in the present model; however, it should be noted that $S_{d\text{-wave}}$ is too small to be consistent with any long-range superconducting order.

APPENDIX C: ADDITIONAL RESULTS AT LOWER T

Figure 7 shows three measurements: kinetic energy, charge structure factor, and total energy, at $\beta = 12/t$, $16/t$, and $20/t$ for $g_{\text{ssh}} = t$ and $1.5t \leqslant g_{\text{hol}} \leqslant 1.8t$. Results for $\beta = 16/t$ overlap well with lower-temperature data $\beta/t = 20$, to within statistical errors, indicating that $\beta = 16/t$ is sufficiently large to use throughout this work in sampling the $T = 0$ phases. We have verified the same is true throughout the phase diagram of Fig. 1.

[1] J. T. Devreese and A. S. Alexandrov, Fröhlich polaron and bipolaron: Recent developments, Rep. Prog. Phys. **72**, 066501 (2009).

[2] C. Franchini, M. Reticcioli, M. Setvin, and U. Diebold, Polarons in materials, Nat. Rev. Mater. **6**, 560 (2021).

[3] J. Bonča, S. A. Trugman, and I. Batistić, Holstein polaron, Phys. Rev. B **60**, 1633 (1999).

[4] M. Berciu and G. L. Goodvin, Systematic improvement of the momentum average approximation for the Green's function of a Holstein polaron, Phys. Rev. B **76**, 165109 (2007).

[5] R. T. Scalettar, N. E. Bickers, and D. J. Scalapino, Competition of pairing and Peierls–charge-density-wave correlations in a two-dimensional electron-phonon model, Phys. Rev. B **40**, 197 (1989).

[6] I. Esterlis, B. Nosarzewski, E. W. Huang, B. Moritz, T. P. Devereaux, D. J. Scalapino, and S. A. Kivelson, Breakdown of the Migdal-Eliashberg theory: A determinant quantum Monte Carlo study, Phys. Rev. B **97**, 140501(R) (2018).

[7] M. Weber and M. Hohenadler, Two-dimensional Holstein-Hubbard model: Critical temperature, Ising universality, and bipolaron liquid, Phys. Rev. B **98**, 085405 (2018).

[8] S. Li and S. Johnston, Quantum Monte Carlo study of lattice polarons in the two-dimensional three-orbital Su–Schrieffer–Heeger model, npj Quantum Mater. **5**, 40 (2020).

[9] C. Feng, H. Guo, and R. T. Scalettar, Charge density waves on a half-filled decorated honeycomb lattice, Phys. Rev. B **101**, 205103 (2020).

[10] B. Xing, W.-T. Chiu, D. Poletti, R. T. Scalettar, and G. Batrouni, Quantum Monte Carlo simulations of the 2D Su-Schrieffer-Heeger model, Phys. Rev. Lett. **126**, 017601 (2021).

[11] C. Feng, B. Xing, D. Poletti, R. Scalettar, and G. Batrouni, Phase diagram of the Su-Schrieffer-Heeger-Hubbard model on a square lattice, Phys. Rev. B **106**, L081114 (2022).

[12] B. Cohen-Stead, K. Barros, R. Scalettar, and S. Johnston, A hybrid Monte Carlo study of bond-stretching electron–phonon interactions and charge order in $BaBiO_3$, npj Comput. Mater. **9**, 40 (2023).

[13] A. Götz, S. Beyl, M. Hohenadler, and F. F. Assaad, Valence-bond solid to antiferromagnet transition in the two-dimensional Su-Schrieffer-Heeger model by Langevin dynamics, Phys. Rev. B **105**, 085151 (2022).

[14] P. Sengupta, A. W. Sandvik, and D. K. Campbell, Peierls transition in the presence of finite-frequency phonons in the one-dimensional extended Peierls-Hubbard model at half-filling, Phys. Rev. B **67**, 245103 (2003).

[15] X. Cai, Z.-X. Li, and H. Yao, Antiferromagnetism induced by bond Su-Schrieffer-Heeger electron-phonon coupling: A quantum Monte Carlo study, Phys. Rev. Lett. **127**, 247203 (2021).

[16] T. Holstein, Studies of polaron motion: Part I. The molecular-crystal model, Ann. Phys. **8**, 325 (1959).

[17] F. Marsiglio, Pairing and charge-density-wave correlations in the Holstein model at half-filling, Phys. Rev. B **42**, 2416 (1990).

[18] M. Vekić, R. M. Noack, and S. R. White, Charge-density waves versus superconductivity in the Holstein model with next-nearest-neighbor hopping, Phys. Rev. B **46**, 271 (1992).

[19] G. G. Batrouni and R. T. Scalettar, Langevin simulations of a long-range electron-phonon model, Phys. Rev. B **99**, 035114 (2019).

[20] M. Hohenadler and G. G. Batrouni, Dominant charge density wave correlations in the Holstein model on the half-filled square lattice, Phys. Rev. B **100**, 165114 (2019).

[21] C. Chen, X. Y. Xu, Z. Y. Meng, and M. Hohenadler, Charge-density-wave transitions of Dirac fermions coupled to phonons, Phys. Rev. Lett. **122**, 077601 (2019).

[22] Y.-X. Zhang, W.-T. Chiu, N. C. Costa, G. G. Batrouni, and R. T. Scalettar, Charge order in the Holstein model on a honeycomb lattice, Phys. Rev. Lett. **122**, 077602 (2019).

[23] O. Bradley, G. G. Batrouni, and R. T. Scalettar, Superconductivity and charge density wave order in the two-dimensional Holstein model, Phys. Rev. B **103**, 235104 (2021).

[24] C. Feng and R. T. Scalettar, Interplay of flat electronic bands with Holstein phonons, Phys. Rev. B **102**, 235152 (2020).

[25] Y. Zhang, C. Feng, R. Mondaini, G. G. Batrouni, and R. T. Scalettar, Charge singlets and orbital-selective charge density wave transitions, Phys. Rev. B **106**, 115120 (2022).

[26] C. Kvande, C. Feng, F. Hébert, G. G. Batrouni, and R. T. Scalettar, Enhancement of charge density wave correlations in a Holstein model with an anharmonic phonon potential, Phys. Rev. B **108**, 075119 (2023).

[27] A. Nocera, J. Sous, A. E. Feiguin, and M. Berciu, Bipolaron liquids at strong Peierls electron-phonon couplings, Phys. Rev. B **104**, L201109 (2021).

[28] M. R. Carbone, A. J. Millis, D. R. Reichman, and J. Sous, Bond-Peierls polaron: Moderate mass enhancement and current-carrying ground state, Phys. Rev. B **104**, L140307 (2021).

[29] C. Zhang, J. Sous, D. R. Reichman, M. Berciu, A. J. Millis, N. V. Prokof'ev, and B. V. Svistunov, Bipolaronic high-temperature superconductivity, Phys. Rev. X **13**, 011010 (2023).

[30] B. Xing, C. Feng, R. Scalettar, G. G. Batrouni, and D. Poletti, Attractive Su-Schrieffer-Heeger-Hubbard model on a square lattice away from half-filling, Phys. Rev. B **108**, L161103 (2023).

[31] A. Tanjaroon Ly, B. Cohen-Stead, S. Malkaruge Costa, and S. Johnston, Comparative study of the superconductivity in the Holstein and optical Su-Schrieffer-Heeger models, Phys. Rev. B **108**, 184501 (2023).

[32] T. P. Devereaux, A. Virosztek, and A. Zawadowski, Charge-transfer fluctuation, d-wave superconductivity, and the B_{1g} Raman phonon in cuprates, Phys. Rev. B **51**, 505 (1995).

[33] S. Johnston, F. Vernay, B. Moritz, Z.-X. Shen, N. Nagaosa, J. Zaanen, and T. P. Devereaux, Systematic study of electron-phonon coupling to oxygen modes across the cuprates, Phys. Rev. B **82**, 064513 (2010).

[34] T. P. Devereaux, T. Cuk, Z.-X. Shen, and N. Nagaosa, Anisotropic electron-phonon interaction in the cuprates, Phys. Rev. Lett. **93**, 117004 (2004).

[35] M. Hohenadler, Interplay of site and bond electron-phonon coupling in one dimension, Phys. Rev. Lett. **117**, 206404 (2016).

[36] X. Xu, D. Sénéchal, and I. Garate, Topological analog of the magnetic bit within the Su-Schrieffer-Heeger-Holstein model, Phys. Rev. B **108**, 214306 (2023).

[37] R. Blankenbecler, D. J. Scalapino, and R. L. Sugar, Monte Carlo calculations of coupled boson-fermion systems. I, Phys. Rev. D **24**, 2278 (1981).

[38] F. F. Assaad, Quantum Monte Carlo methods on lattices: The determinantal approach, in *Quantum Simulations of Complex Many-Body Systems: From Theory to Algorithms*, edited by J. Grotendorst, D. Marx, and A. Muramatsu, Lecture Notes NIC Series Vol. 10 (John von Neumann Institute for Computing, Jülich, 2002), pp. 99–156.

[39] S. Johnston, E. A. Nowadnick, Y. F. Kung, B. Moritz, R. T. Scalettar, and T. P. Devereaux, Determinant quantum Monte Carlo study of the two-dimensional single-band Hubbard-Holstein model, Phys. Rev. B **87**, 235133 (2013).

[40] E. Y. Loh, J. E. Gubernatis, R. T. Scalettar, S. R. White, D. J. Scalapino, and R. L. Sugar, Sign problem in the numerical simulation of many-electron systems, Phys. Rev. B **41**, 9301 (1990).

[41] M. Troyer and U.-J. Wiese, Computational complexity and fundamental limitations to fermionic quantum Monte Carlo simulations, Phys. Rev. Lett. **94**, 170201 (2005).

[42] R. Mondaini, S. Tarat, and R. T. Scalettar, Quantum critical points and the sign problem, Science **375**, 418 (2022).

[43] J. K. Freericks, M. Jarrell, and D. J. Scalapino, Holstein model in infinite dimensions, Phys. Rev. B **48**, 6302 (1993).

[44] N. C. Costa, T. Blommel, W.-T. Chiu, G. Batrouni, and R. T. Scalettar, Phonon dispersion and the competition between pairing and charge order, Phys. Rev. Lett. **120**, 187003 (2018).

[45] B. Cohen-Stead, N. C. Costa, E. Khatami, and R. T. Scalettar, Effect of strain on charge density wave order in the Holstein model, Phys. Rev. B **100**, 045125 (2019).

[46] B. Nosarzewski, E. W. Huang, P. M. Dee, I. Esterlis, B. Moritz, S. A. Kivelson, S. Johnston, and T. P. Devereaux, Superconductivity, charge density waves, and bipolarons in the Holstein model, Phys. Rev. B **103**, 235156 (2021).

[47] M. V. Araújo, J. P. de Lima, S. Sorella, and N. C. Costa, Two-dimensional t-t' Holstein model, Phys. Rev. B **105**, 165103 (2022).

[48] D. Baeriswyl, Theoretical aspects of conducting polymers: Electronic structure and defect states, in *Theoretical Aspects of Band Structures and Electronic Properties of Pseudo-One-Dimensional Solids* (Springer, Berlin, 1985), pp. 1–48.

[49] V. J. Emery, Theory of the one-dimensional electron gas, in *Highly Conducting One-Dimensional Solids*, edited by J. T. Devreese, R. P. Evrard, and V. E. van Doren (Springer US, Boston, 1979), pp. 247–303.

[50] M. Nakamura, Tricritical behavior in the extended Hubbard chains, Phys. Rev. B **61**, 16377 (2000).

[51] S. Ejima and S. Nishimoto, Phase diagram of the one-dimensional half-filled extended Hubbard model, Phys. Rev. Lett. **99**, 216403 (2007).

[52] N. C. Costa, K. Seki, S. Yunoki, and S. Sorella, Phase diagram of the two-dimensional Hubbard-Holstein model, Commun. Phys. **3**, 80 (2020).

[53] P. M. Dee, K. Nakatsukasa, Y. Wang, and S. Johnston, Temperature-filling phase diagram of the two-dimensional Holstein model in the thermodynamic limit by self-consistent Migdal approximation, Phys. Rev. B **99**, 024514 (2019).